International Journal of Thermal Sciences 49 (2010) 1147–1155

Contents lists available at ScienceDirect

International Journal of Thermal Sciences

journal homepage: www.elsevier.com/locate/ijts

An analytical solution for thermocapillary-driven convection of superimposed fluids at zero Reynolds and Marangoni numbers

Bhushan Pendse, Asghar Esmaeeli*

Department of Mechanical Engineering & Energy Processes, Southern Illinois University, Carbondale, IL 62901, USA

ARTICLE INFO

Article history:
Received 19 August 2009
Received in revised form
6 February 2010
Accepted 8 February 2010
Available online 12 March 2010

Keywords:
Thermocapillary
Patterned wall
Creeping flow
Microchannel
Interface deformation

ABSTRACT

This study aims to investigate thermocapillary-driven convection in two superimposed fluids in zero gravity. The fluids occupy the space between the walls of a horizontal microchannel which is heated from below by imposing the top wall to a uniform temperature and the bottom wall to a sinusoidal temperature that is higher (on the average) than the temperature of the top wall. The goal is to mimic thermocapillary convection as a result of the variation of the heights of the fluids along the microchannel and to explore the parameters that affect the fluid flow and interface deformation. This is achieved by solving the equations of conservation of mass and momentum and the balance of thermal energy and negligible analytically in both fluids, in the limit of creeping flow regime and negligible convection of heat. It is shown that the induced flow is characterized by periodic convection cells whose period is the same as the period of the imposed temperature field and extend from the interface to the walls in the vertical direction. The flow strength depends on the relative thicknesses of the fluid layers and the ratio of material properties. The maximum flow strength is achieved at a relative thickness that is set by the competition between the thermal and hydrodynamic effects. An estimate of the interface deformation is provided and it is shown that the sense of interface deformation is set by the relative thickness of the fluid layers and the viscosity ratio.

1. Introduction

When the interface separating two fluids is exposed to a temperature gradient, the variation of the surface tension at the interface with the temperature will lead to an interfacial shear force along the interface that sets the fluids to motion. For most fluids the surface tension is a decreasing function of the temperature (see, for example, [1]). Therefore, the fluids typically move from the regions of higher temperature, where the surface tension is low, to the colder regions, where the surface tension is high. This phenomenon is known as thermocapillary (or Marangoni) convection and has been known for decades. See, for example, [2] and [3].

Thermocapillary forces provide a particularly attractive means for manipulation of continuous fluid streams or discrete fluid samples, such as bubbles and drops, in applications involving microgravity [4] or microdevices [5], where the surface forces become increasingly dominant as the dimensions of the device are decreased. These forces, on the other hand, are responsible for heat transfer failure in some technologically important applications as a result of interface instability. One such example is the spontaneous film rupture and dry out in micro-evaporators that are used in numerous industries for thermal management of electronic devices and MEMS. Here, even if the heated wall is assumed to be isothermal and flat, slight perturbations in the liquid film thickness can lead to thermocapillary convection that drives the fluid from the region of lower film thickness (higher interface temperature) to the region of higher film thickness (lower interface temperature). In the absence of stabilizing effect, the instability leads to film rupture; see, for example, [6–8].

In this study we are interested in exploring the thermocapillary-driven flow of continuous fluid streams in microchannels and in zero gravity as a result of the variations of the film thicknesses along the channel or due to micropatterning of the heated wall. Our goal is to formulate this problem analytically and to develop a simple closed form solution. This problem finds applications in boiling and condensation in microchannels with flat or micropatterned walls. The patterned structure has been the focus of attention in microdevices for variety of reasons, ranging from understanding the effect of surface irregularities on fluid flow [9], to surface patterning to produce three-dimensional flows in simple channel shapes [10], and up to the enhancement of evaporation rate using patterned walls [11]. In the presence of a temperature gradient, the possibility

* Corresponding author. Tel.: +1 618 453 7001; fax: +1 618 453 7685.
E-mail address: esmaeeli@engr.siu.edu (A. Esmaeeli).

1290-0729/$ – see front matter © 2010 Elsevier Masson SAS. All rights reserved.
doi:10.1016/j.ijthermalsci.2010.02.003

Nomenclature

a	height of the upper fluid
b	height of the lower fluid
l	channel length
$w = a + b$	channel height
c	specific heat
k	thermal conductivity; also wave number $k = 2\pi/l$
p	pressure
$Pr = \mu c/k$	the Prandtl number
$Ma = u_s a/\alpha$	the Marangoni number
$Re = u_s a/\nu$	the Reynolds number
T	temperature field
$\boldsymbol{u}$	velocity field
$u_s = (\lvert\sigma_T\rvert \Delta T/\mu_b)(b/l)$	velocity scale

Greek Symbols

μ	dynamic viscosity
ρ	density
σ	surface tension
τ	hydrodynamic shear stress
κ	curvature
ν	kinematic viscosity
α	thermal diffusivity; also $\alpha = ka$
β	kb
ϕ	linear temperature field
θ	perturbation temperature field
$\tilde{\mu} = \mu_a/\mu_b$	viscosity ratio
$\tilde{k} = k_a/k_b$	heat conductivity ratio
ψ	streamfunction
$\Delta T \sim (T_h + T_0) - (T_h - T_0) \sim T_0$	characteristic temperature difference

subscripts

a	above
b	below

superscripts

a	above
b	below

of thermocapillary-driven flow is higher in microdevice with patterned surfaces compared to those with flat surfaces. Rather than considering variations in the thickness of the fluid layers or variations in the elevation of the heated wall as a result of micropatterning, we consider a horizontal channel with flat surfaces which is exposed to a uniform temperature at the upper wall and a sinusoidal temperature along the lower wall. This way the variation of the temperature along the lower wall can be interpreted as the variation in the elevation of a micropatterned isothermal heater or the variation of the fluid film thickness. This simplification helps present an analytical closed form solution for the problem and leads to results that will capture the essence of the actual phenomenon. The heat conduction equation and creeping flow equations are solved in both fluids and the effect of controlling parameters such as ratio of the material properties and the film thickness on the induced convection and interface deformation is studied.

2. Problem setup

Consider two superimposed planar fluids as shown in Fig. 1. The heights of the lower and upper fluids are b and a, respectively, but the fluids are of infinite extension in the horizontal direction. The physical properties of the fluids are their densities, ρ_b, ρ_a, viscosities, μ_b, μ_a, and heat conductivities, k_b, k_a. The surface tension at the interface of the two fluids is σ. Here, the subscripts/superscripts b and a denote the parameters associated with the fluids below and the above of the interface, respectively. The temperature variations in the present study are considered to be small enough so that the thermophysical properties of each fluid to remain constant, with the exception of surface tension. The temperature of the lower and upper plates are

$$T^b(x, -b) = T_h + T_0 \cos(kx)$$

and

$$T^a(x, a) = T_c,$$

respectively, where $T_h > \mathrm{Tc} > T_0 > 0$, l is the channel length, and $k = 2\pi/l$ is a wave number. The above temperature boundary conditions establishes a temperature field that is periodic in the horizontal direction with a period of l. Therefore, it is only sufficient to focus on the solution in one period; i.e., $-l/2 < x < l/2$.

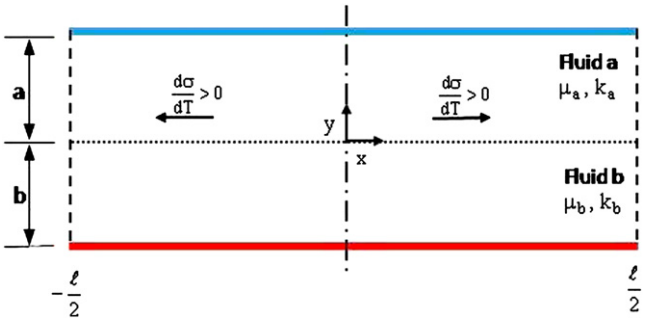

Fig. 1. The geometric setup depicting two immiscible fluids in a microchannel. The temperature of the lower and upper plates are $T^b(x, -b) = T_h + T_0 \cos(kx)$ and $T^a(x, a) = T_c$, respectively, where $T_h > \mathrm{Tc} > T_0$ and $k = 2\pi/l$ is a wave number. The gravity is zero.

To find the governing nondimensional numbers, it is imperative to recognize first the natural velocity and the length scales. This problem does not have a natural velocity scale. However, a velocity scale can be constructed based on the fact that the fluid flow is established as a result of balance of surface tension gradient along the interface, $d\sigma/dx$, and the viscous shear stress at the interface, τ_μ. The surface tension gradient scales as $(d\sigma/dT)(\Delta T/l)$, where $\Delta T \sim (T_h + T_0) - (T_h - T_0) \sim T_0$ is the characteristic temperature difference. The viscous shear stress τ_μ scales as $\mu u_s/l_s$, where l_s is a length scale associated with the fluids depths and u_s is the velocity scale. Here, we have chosen to use the properties of the lower fluid to nondimensionalize and to account for the influence of the upper fluid using the ratio of material properties. Setting $|\sigma_T|(\Delta T/l) \sim \mu_b u_s/b$, results in $u_s = (|\sigma_T|\Delta T/\mu_b)(b/l)$, where $\sigma_T = d\sigma/dT|_0$ is a characteristic surface tension gradient. Nondimensionalization of the controlling parameters leads to the Reynolds number $Re = u_s b/\nu_b$, the Marangoni number $Ma = u_s b/\alpha_b$, and the capillary number $Ca = \mu_b u_s/\sigma_0$ as the primary nondimensional numbers of this problem. Here, σ_0 is the surface tension at a reference temperature, $\nu = \mu/\rho$, and $\alpha = k/\rho c$. The ratio of material properties, $\tilde{\rho} = \rho_a/\rho_b$ and $\tilde{\mu} = \mu_a/\mu_b$, $\tilde{k} = k_a/k_b$, and $\tilde{c} = c_a/c_b$, and the nondimensional thickness of the lower layer, $\tilde{b} = b/l$ or b/w, provide a secondary set of nondimensional numbers.

In this study, we are interested in situations where convective transport of momentum and energy is negligible, and interface remains flat. This translates to $Re << 1$, $Ma << 1$, and $Ca << 1$, respectively. This range of nondimensional numbers can be realized, for example, by considering a channel of length $l = 100$ μm and height $w = 50$ μm, and a temperature gradient of $|\nabla T| = 1$ K/mm, which is typical of the experiments. For common fluids, a surface tension gradient of $\sigma_T = -10^{-4}$ N/m.K, a surface tension of $\sigma_0 = 0.3$ N/m, and a kinematic viscosity of $\nu_b = 10^{-5}$ m^2/s serve as typical values. The typical values of $\alpha_b = 10^{-5}$ m^2/s and 10^{-8} m^2/s, are for the liquids and gases, respectively. The above characteristic values result in *Re*, *Ma*, and *Ca* numbers that are typically $O(0.01)$ or at most $O(1)$. Since the analysis is for creeping flow regime, the density ratio does not play a role, and since the flow is at a steady state, the results are independent of the heat capacity ratio $\tilde{c} = c_a/c_b$. Therefore, the governing nondimensional numbers of this flow are the thermal conductivity ratio $\tilde{k}$, the viscosity ratio $\tilde{\mu}$, and the nondimensional thickness of the lower fluid layer $\tilde{b}$.

3. Governing equations

The governing equations for this problem are the conservation of mass and momentum, and the balance of thermal energy at steady state. These equations are valid for each fluid and are coupled together through jump conditions at the interface. The fluids are considered incompressible, immiscible, and Newtonian. Assuming $Re << 1$ and $Ma << 1$, it is possible to ignore the convective transport of momentum and energy. This simplifies greatly the momentum and the energy equation as these equations become linear. Assuming further that $Ca << 1$, the interface can be considered to remain flat. The mass conservation, accounting for incompressibility condition, simplifies to

$$\nabla\cdot\mathbf{u} = 0, \tag{1}$$

the momentum equation yields

$$-\nabla p + \mu\nabla^2\mathbf{u} = 0, \tag{2}$$

and the balance of energy equation simplifies to

$$\nabla^2 T = 0, \tag{3}$$

where $\nabla^2 = \partial^2/\partial x^2 + \partial^2/\partial y^2$. In addition to the above equations, an equation of state is needed to relate the surface tension to the temperature. The dependency of surface tension on temperature is generally nonlinear, however, for small temperature variation, $\Delta T/T_h << 1$, it is possible to consider a linear relation between the surface tension and the temperature

$$\sigma(T) = \sigma_{\max} + \sigma_T(T - T_{\min}), \tag{4}$$

where

$$\sigma_T = -\frac{\sigma_{\max} - \sigma_{\min}}{T_{\max} - T_{\min}}, \quad T_{\max} = T_h + T_0, \quad \text{and} \quad T_{\min} = T_c.$$

Rather than solving the momentum equation directly, it is more convenient to work with equation for the streamfunction ψ; i.e.,

$$\nabla^4\psi = 0, \tag{5}$$

where $\nabla^4 = \nabla^2(\nabla^2)$ is the biharmonic operator.

4. Solution of the energy equation

The energy equation is decoupled from the momentum equation, but, the momentum equation depends on the energy equation through the surface tension term in the tangential momentum jump condition. Since the differential equation is homogeneous and the temperature is periodic in the x direction, separation of variables can be used to solve for the temperature, provided the temperature field $T(x, y)$ is written as

$$T^i(x,y) = \theta^i(x,y) + \phi^i(y); \quad i = a, b, \tag{6}$$

where $\phi^i(y)$ is a linear temperature field and $\theta^i(x, y)$ is a perturbation temperature field. Substitution of T^i in the energy equation and the associated boundary conditions result in

$$\nabla^2\theta^i = 0; \quad i = a, b, \tag{7}$$

and

$$\frac{d^2\phi^i}{dy^2} = 0; \quad i = a, b, \tag{8}$$

and the following boundary conditions for θ^i and ϕ^i:

i) The temperature is specified at the lower wall:

$$\theta^b(x,-b) = T_0\cos(kx); \quad \phi^b(-b) = T_h$$

ii) The temperature is specified at the upper wall:

$$\theta^a(x,a) = 0; \quad \phi^a(a) = T_c$$

iii) The temperature must be continuous at the interface:

$$\theta^a(x,0) = \theta^b(x,0); \quad \phi^a(0) = \phi^b(0)$$

iv) The heat flux must be continuous at the interface:

$$k_b\frac{\partial\theta^b}{\partial y}\bigg|_{y=0} = k_a\frac{\partial\theta^a}{\partial y}\bigg|_{y=0}; \quad k_b\frac{d\phi^b}{dy}\bigg|_{y=0} = k_a\frac{d\phi^a}{dy}\bigg|_{y=0}.$$

The solution for $\phi(y)$ yields in

$$\phi^b(y) = \frac{k_a(T_c - T_h)y + T_c k_a b + T_h k_b a}{ak_b + bk_a}, \tag{9}$$

and

$$\phi^a(y) = \frac{k_b(T_c - T_h)y + T_c k_a b + T_h k_b a}{ak_b + bk_a}, \tag{10}$$

in the lower and upper fluid, respectively. The suggested solution for θ is of the form $\theta(x, y) = X(x)Y(y)$. Substitution for θ in the energy equation leads to $X'' + n^2X = 0$ and $Y'' - n^2Y = 0$, where prime denotes derivation with respect to x or y, and n is a constant to be determined. The solution of the above ODEs are

$$X(x) = A\cos(nx) + B\sin(nx),$$

and

$$Y(y) = C\cos h(ny) + D\sin h(ny),$$

where A, B, C, and D are constants to be determined from the boundary conditions. The imposed temperature boundary condition on the lower plate suggests that the sin term should be dropped from the expression for $X(x)$ and also $n = k$. This results in the following temperature distributions

$$\theta^b(x,y) = \left[A_1^b \cos h(ky) + A_2^b \sin h(ky)\right]\cos(kx), \tag{11}$$

and

$$\theta^a(x,y) = \left[A_1^a \cos h(ky) + A_2^a \sin h(ky)\right]\cos(kx), \tag{12}$$

in the lower and upper fluid, respectively. Notice that A_1^b, A_2^b, A_1^a, and A_2^a are new constants which results from combining of constants $A - D$. The solution of the algebraic equations associated with the above boundary conditions results in

$$A_1^a = A_1^b = T_0 \sin h(\alpha) f(\alpha,\beta,\tilde{k}),$$

$$A_2^a = -T_0 \cos h(\alpha) f(\alpha,\beta,\tilde{k}); \quad A_2^b = -T_0 \tilde{k} \cos h(\alpha) f(\alpha,\beta,\tilde{k}),$$

where $\alpha = ka$, $\beta = kb$, and

$$f(\alpha,\beta,\tilde{k}) = \left[\tilde{k}\sin h(\beta)\cos h(\alpha) + \sin h(\alpha)\cos h(\beta)\right]^{-1}. \tag{13}$$

Substitution for the constants in equations (11) and (12) results in the electric potential in the lower fluid

$$\theta^b(x,y) = T_0 f(\alpha,\beta,\tilde{k})\left[\sin h(\alpha)\cos h(ky) - \tilde{k}\sin h(ky)\cos h(\alpha)\right]\cos(kx), \tag{14}$$

and the upper fluid

$$\theta^a(x,y) = T_0 f(\alpha,\beta,\tilde{k}) \sin h(\alpha - ky)\cos(kx). \tag{15}$$

The variation of the interface temperature is a key parameter in setting the strength and direction of the flow field. As can be seen from equations (9)–(10) and (14)–(15), the ratio of the thermal conductivities of the fluids plays a major role in this parameter. Fig. 2 shows equispaced contours of temperature field for three different conductivity ratios; $\tilde{k} = 0.5$, 0.01, and 100; i.e., top, middle, and bottom frame, respectively. These conductivity ratios represent, respectively, a liquid/liquid system such as silicon oil and water, a liquid/gas system such as water/air, and a phase-reversed system. Here, the thicknesses of the fluid layers are equal. For all the cases, the direction of heat transfer is predominantly upward, however, some heat transfer is also taking place from the middle to the sides. For $\tilde{k} = 0.5$ (top frame), the slopes of the contour lines for both fluids at the interface are nearly equal, reflecting the fact that the thermal conductivities of the fluids are close. For $\tilde{k} = 0.01$ (middle frame) on the other hand, the slopes of the contour lines at the interface are remarkably different at both sides. Here, the slopes of the contour lines approaching from the lower fluid are normal to the interface, reflecting the fact that heat transfer in the vertical direction is nearly zero at the interface, because of the very low thermal conductivity of the upper fluid. For $\tilde{k} = 100$ (bottom frame), the temperature is essentially uniform in the upper fluid and as a result, the temperature gradient nearly vanishes in this fluid. Therefore, the interface temperature becomes nearly the same as the temperature of the upper wall. Here, as opposed to $\tilde{k} = 0.01$ case, the temperature gradient along the interface is zero. As a result, the contour lines near the interface conform to its shape. The heat flux vectors confirm further the above observations. Judging by the scale of the vectors in the upper and the lower fluids, it is seen that the heat transfer rate in the upper fluid is nearly zero for $\tilde{k} = 0.01$ and it is the highest for $\tilde{k} = 100$. Fig. 3, which shows the variation of the perturbed temperature at $x = 0$ along the channel height, summarizes the above observations.

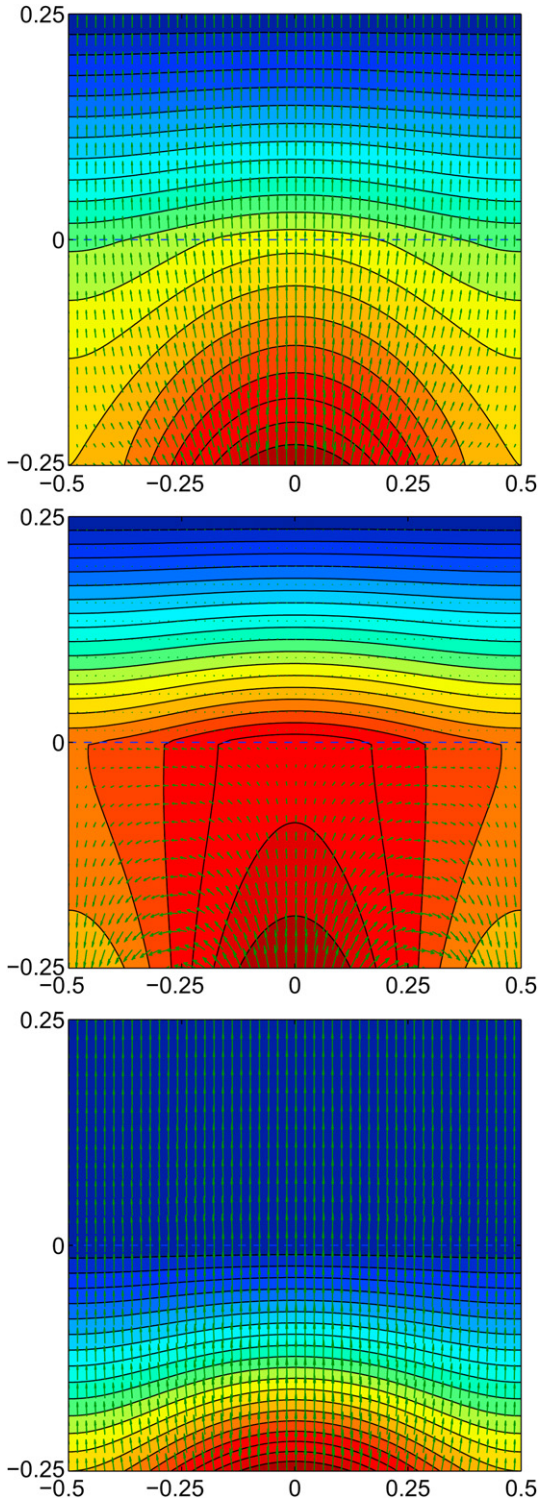

Fig. 2. Temperature contours and heat flux vectors for fluid systems with heat conductivity ratios of $\tilde{k} = 0.5$ (top frame), 0.01 (middle frame), and 100 (bottom frame), respectively. Here, $w/l = 0.5$ and $a/l = b/l = 0.25$.

5. Solution of the streamfunction equation

Similar to the solution of the perturbed temperature $\theta(x, y)$, the suggested solution for ψ is of the form $\psi(x, y) = X(x)Y(y)$. Before substitution for $\psi(x, y)$ in the biharmonic equation, however, it is possible to recognize the functional structure of $X(x)$ from the balance of hydrodynamic shear stress at the interface:

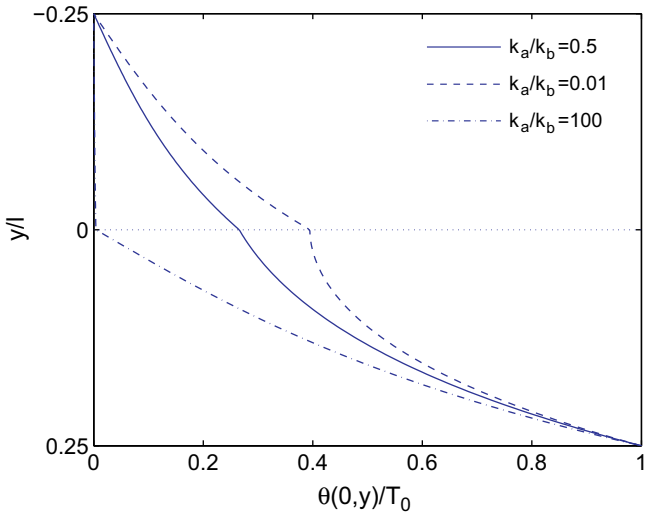

Fig. 3. Variation of the perturbation temperature, $\theta(0,y)/T_0$, with y/l for the three cases discussed in Fig. 2.

$$\left(\tau_{xy}^b - \tau_{xy}^a\right)\Big|_{y=0} = \frac{d\sigma}{dT}\frac{\partial T}{\partial x}\Big|_{y=0}, \tag{16}$$

where

$$\tau_{xy} = \mu\left(\frac{\partial u}{\partial y} + \frac{\partial v}{\partial x}\right).$$

Since $d\sigma/dT$ = constant and $\partial T/\partial x|_{y=0} \sim \sin(kx)$, therefore, $\tau_{xy} \sim \sin(kx)$, which suggests that $\psi = f(y)\sin(kx)$. To find $f(y)$, ψ is substituted in equation (5) which results in

$$f'''' - 2k^2 f'' + k^4 f = 0.$$

The suggested solution for the above equation is e^{my}, where m is a constant to be determined. Here, the characteristic equation for the above ODE is $(m^2 - k^2)^2 = 0$ which results in $m = \pm k$. Because of the double roots, the four independent solutions for f are e^{ky}, ye^{ky}, e^{-ky}, and ye^{-ky}. Since the domain is finite in the vertical direction, it is more appropriate to present the results in terms of hyperbolic functions. This yields the following expressions for stream functions in the lower fluid

$$\psi^b = U_{\max}\left[\left(C_1^b + C_2^b y\right)\cos h(ky) + \left(C_3^b + C_4^b y\right)\sin h(ky)\right]\sin(kx) \tag{17}$$

and the upper one

$$\psi^a = U_{\max}\left[(C_1^a + C_2^a y)\cos h(ky) + (C_3^a + C_4^a y)\sin h(ky)\right]\sin(kx). \tag{18}$$

Here, C_i^b and C_i^a are eight unknown constants to be determined, where $i = 1$–4. We have also introduced a new unknown $U_{\max}$ which is the maximum interface velocity and is determined as part of the solution. The unknowns are determined using the following boundary condition:

i) No-slip, no-through flow boundary condition at the lower wall:

$$u^b(x,-b) = 0, \quad v^b(x,-b) = 0.$$

ii) No-slip, no-through flow boundary condition at the upper wall:

$$u^a(x,a) = 0, \quad v^a(x,a) = 0.$$

iii) Continuity of the tangential component of the velocity at the interface:

$$u^b(x,0) = U_{\max}\sin(kx), \quad u^a(x,0) = U_{\max}\sin(kx).$$

iv) No-through flow boundary condition at the interface:

$$v^b(x,0) = 0, \quad v^a(x,0) = 0.$$

v) Balance of shear stress:

$$\mu_b\frac{\partial u^b}{\partial y}\Big|_{y=0} - \mu_a\frac{\partial u^a}{\partial y}\Big|_{y=0} = \sigma_T\frac{\partial T}{\partial x}\Big|_{y=0}.$$

Notice that in the above equation we have dropped the $\partial v/\partial x$ term from the hydrodynamic shear stress because $v = 0$ at the interface according to (*iii*). The first eight boundary conditions determines C_i^a and C_i^b, $i = 1$–4, and the last boundary condition determines $U_{\max}$. This results in

$$C_1^a = C_1^b = 0,$$

$$C_2^a = \frac{\sin h^2(\alpha)}{\sin h^2(\alpha) - \alpha^2}; \quad C_2^b = \frac{\sin h^2(\beta)}{\sin h^2(\beta) - \beta^2},$$

$$C_3^a = \frac{-a\alpha}{\sin h^2(\alpha) - \alpha^2}; \quad C_3^b = \frac{-b\beta}{\sin h^2(\beta) - \beta^2},$$

$$C_4^a = -\frac{\sin h(2\alpha) - 2\alpha}{2\left(\sin h^2(\alpha) - \alpha^2\right)}; \quad C_4^b = \frac{\sin h(2\beta) - 2\beta}{2\left(\sin h^2(\beta) - \beta^2\right)},$$

and

$$U_{\max} = -\left(\frac{T_0\sigma_T}{\mu_b}\right)g(\alpha,\beta,\tilde{k})h(\alpha,\beta,\tilde{\mu}), \tag{19}$$

where

$$g(\alpha,\beta,\tilde{k}) = \sin h(\alpha) f(\alpha,\beta,\tilde{k}), \tag{20}$$

and

$$h(\alpha,\beta,\tilde{\mu}) = \frac{\left(\sin h^2(\alpha) - \alpha^2\right)\left(\sin h^2(\beta) - \beta^2\right)}{\tilde{\mu}\left(\sin h^2(\beta) - \beta^2\right)\left(\sin h(2\alpha) - 2\alpha\right) + \left(\sin h^2(\alpha) - \alpha^2\right)\left(\sin h(2\beta) - 2\beta\right)}. \tag{21}$$

Substitution of these constants in equations (17) and (18) yields the streamfunction in the lower fluid

$$\frac{\psi^b}{U_{\max}/k} = \frac{1}{\sin h^2(\beta) - \beta^2}\left\{\sin h^2(\beta)(ky)\cos h(ky) - \frac{1}{2}\left[2\beta^2 - (\sin h(2\beta) - 2\beta)(ky)\right]\sin h(ky)\right\}\sin(kx), \quad (22)$$

and the upper fluid

$$\frac{\psi^a}{U_{max}/k} = \frac{1}{\sin h^2(\alpha) - \alpha^2}\left\{\sin h^2(\alpha)(ky)\cos h(ky) - \frac{1}{2}\left[2\alpha^2 + (\sin h(2\alpha) - 2\alpha)(ky)\right]\sin h(ky)\right\}\sin(kx), \quad (23)$$

Fig. 4 shows a few equispaced streamline contours along with the velocity vectors for a case where $\tilde{k} = 0.01$ and $\tilde{\mu} = 0.1$ with relative fluid layer thicknesses of $a/b = 3$, 1, and 1/3. For all the cases, the fluid flow consists of four counter-rotating vortices that divide the domain into four parts. The sense of fluid circulation is set by the temperature gradient at the interface. The interface temperature, $T(x, 0)$, behaves as $\cos(kx)$, and the surface tension gradient, $d\sigma/dx$, behaves as $\sin(kx)$, as predicted by equation (4). This leads to a shear force at the interface that is from the center to the left (right) in the left (right) half of the domain. The fluids are set to motion by this shear force and move from the middle toward the right and the left. Since the domain is periodic in the horizontal direction, the velocities of the left-moving and right-moving fluids decreases as they approach their images in the adjacent periodic domains. As a result, the fluid is forced to turn upward (downward) in the upper (lower) half of the domain. The upward and the downward flow streams, however, slow down as they approach the walls and turn around near the walls and move parallel to the walls from the sides toward the middle. The horizontal fluid streams are forced to turn upward (downward) in the lower (upper) half as they approach each other from the sides to the center. This results in the formation of the circulation patterns seen in the figure.

The coordinates of the cores of the vortices, (x_c, y_c), can be determined considering the fact that at the cores both components of the velocity are zero. x_c is set by the periodicity of the flow and can be easily found by inspection of the streamlines where it is seen that the streamlines are quite horizontal along the lines $x/l = \pm 1/4$. The horizontal separation distance between vortices is always 1/2 and, therefore, independent of the flow parameters. y_c, on the other hand, depends on the thickness of the fluid layers and can be found by setting $u(x_c, y)$ to zero. Surprisingly, however, y_c is independent of the viscosities of the fluids. The vertical coordinates of the cores, measured from the interface, are about a third of the layer thickness in the middle frame. It moves closer to the interface when the thickness of the fluid layer is decreased and vice versa. It appears that the vertical separation distance between the centers of vortices is about one third of the channel height.

The flow strength is characterized by $U_{\max}$ which is proportional to $g(\alpha, \beta, \tilde{k}) \times h(\alpha, \beta, \tilde{\mu})$. For a fluid system with $\tilde{k} = 0.01$ and $\tilde{\mu} = 0.1$, the variation of $g \times h$ with the nondimensional thickness of the lower layer $\tilde{b} = b/w$ is shown in Fig. 5*a*. Here, to aid understanding of the results, b is measured with respect to a coordinate system attached to the lower left corner of the channel and is nondimensionalized with the separation distance between the walls, $w = a + b$. It is seen that $g \times h$ starts from zero, reaches a maximum, and gradually decays to zero. To find out the factors that determine the thickness where the velocity is maximum, in Fig. 5*b* and *c* we plot g and h as a function of nondimensional thickness of the lower layer with $\tilde{k}$ and $\tilde{\mu}$ as parameters. Fig. 5*b* shows that for a given $\tilde{b}$, g decreases as $\tilde{k}$ increases, and for a given $\tilde{k}$, g decreases with an increase in $\tilde{b}$. The reasons for this behavior are, respectively, that the temperature gradient along the interface decreases as the heat conductivity of the upper fluid increases, and the fact that heat transfer from the heated wall decreases as the thermal conduction resistance increases with an increase in the thickness of the lower fluid layer. Fig. 5*c* shows that for a given $\tilde{b}$, h decreases as $\tilde{\mu}$ increases, and for a given $\tilde{\mu}$, h starts from zero,

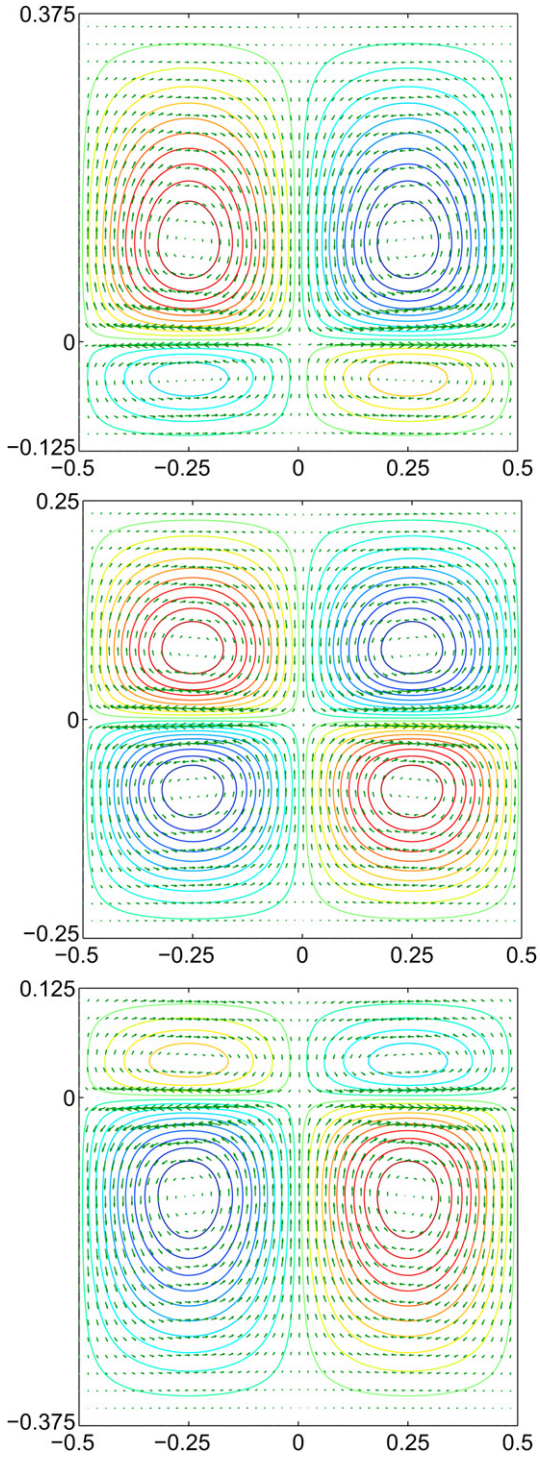

Fig. 4. Streamline contours and velocity vectors for two fluid systems with relative thickness of $a/b = 3$ (top frame), 1 (middle frame), and 1/3 (bottom frame), respectively. Here, $\tilde{k} = 0.01$, $\tilde{\mu} = 0.1$, and $w/l = 0.5$.

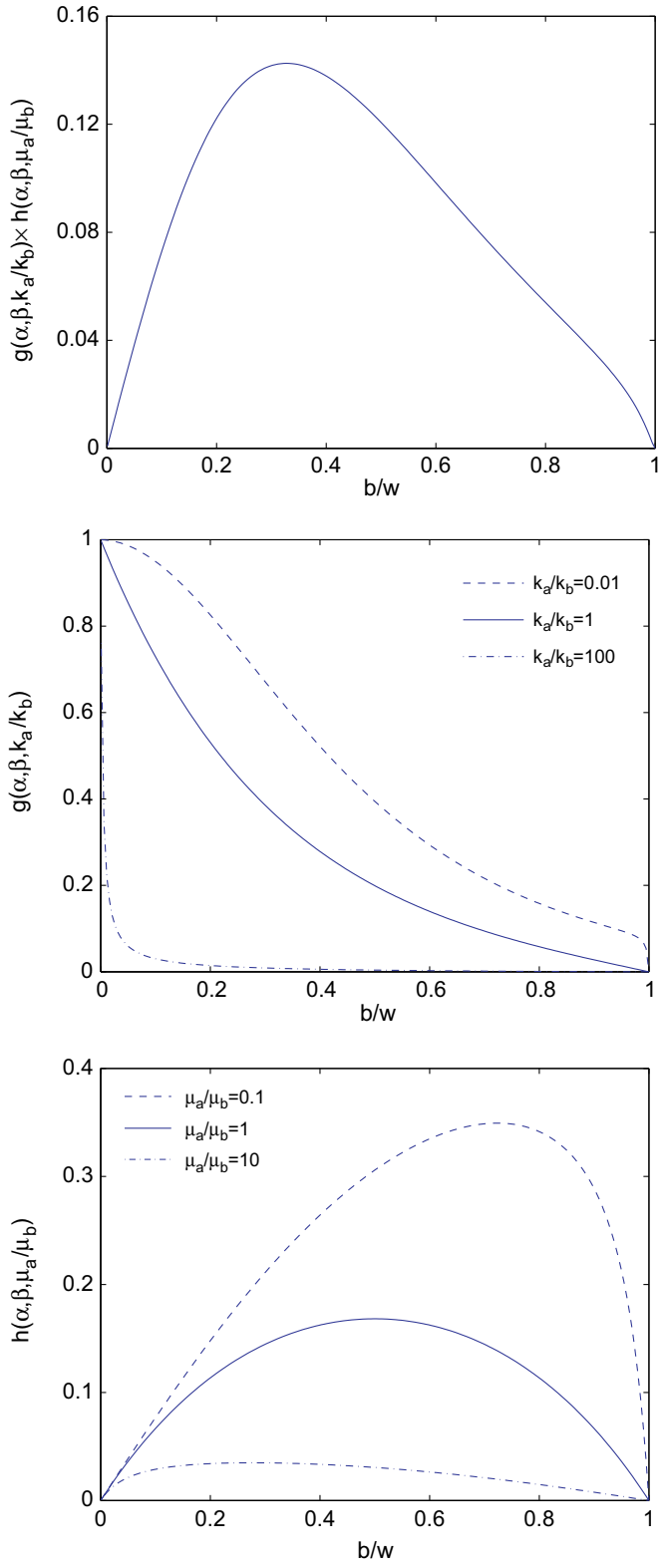

Fig. 5. Variation of $g(\alpha,\beta,\tilde{k}\times h(\alpha,\beta,\tilde{\mu}$ (top frame), g (middle frame), and h (bottom frame) versus the nondimensional thickness of the lower layer. For the first frame, $\tilde{k}=0.01$ and $\tilde{\mu}=0.1$. Here, b is measured with respect to a coordinate system attached to the lower left corner of the channel and w is nondimensionalized with the separation distance between the walls.

reaches a maximum, and gradually decays to zero. The figure shows that h becomes maximum when the more viscous fluid has also the larger thickness compared to that of the less viscous fluid. This can be inferred from the shift in the maximum from the left to the right as $\tilde{\mu}$ is decreased. It is seen that when both fluids have the same viscosity, h will be maximum when both layers have the same thickness. This behavior suggests that the hydrodynamic shear stresses τ_{xy} immediately across the interface should be uniform so that $U_{\max}$, and therefore h, scales as δ/μ, where δ is the vertical distance over which the horizontal velocity drops from $U_{\max}$ to zero. This argument can be further backed by considering the shear stress balance at the interface:

$$\frac{\sigma_T \Delta T}{l} \sim \frac{\mu_a U_{\max}}{\delta_a} + \frac{\mu_b U_{\max}}{\delta_b}.$$

Here, δ_a and δ_b are the vertical coordinates of the cores of the vortices in the upper and the lower layers, measured from the interface, where the horizontal velocity comes to halt. Considering the fact that $\delta_a \sim a$ and $\delta_b \sim b$, and solving for $U_{\max}$ yields

$$U_{\max} \sim \frac{\sigma_T \Delta T/l}{\mu_a/a + \mu_b/b}.$$

This equation suggests that for $\mu_a > \mu_b$ or $\mu_a < \mu_b$, the denominator will be minimum when $a > b$ or $a < b$, respectively. Fig. 6, which shows the nondimensional horizontal velocity as a function of y/w at $x/l = 1/4$ and $3/8$, supports the above argument. Here, $\tilde{k} = 0.5$, $\tilde{\mu} = 0.5$, and $a/l = b/l = 0.25$. $x/l = 1/4$ and $x/l = 3/8$ represent, respectively, vertical lines that passes through the core of the vortices and midway between the core and the channel end. The open circles mark the points with zero and maximum horizontal velocities. For both cases, it is clearly seen that the horizontal velocity varies nearly linearly from a maximum at the interface to zero near the cores of the vortices. In summary, as can be inferred from Fig. 5, the thickness at which $U_{\max}$ becomes maximum is set by the thickness for which the product of g and h becomes maximum. Since g and h depend, respectively, on $\tilde{k}$ and $\tilde{\mu}$, this

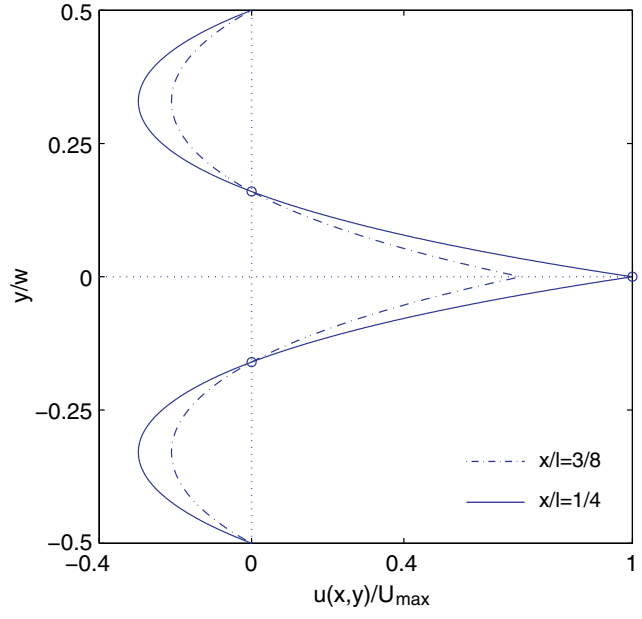

Fig. 6. $u(x, y)/U_{\max}$ as a function of y/w at $3l/8$ and $l/4$. w is the separation distance between the walls. Here, $\tilde{k} = 0.5$, $\tilde{\mu} = 0.5$, and $a/l = b/l = 0.25$.

means that this thickness is determined by the competition between the thermal and hydrodynamic effects.

6. Interface deformation

The analysis so far was based on the premise that the interface remains flat. However, the interface is likely to deform by the normal stresses. For small deformation, it is possible to calculate distortion from planar shape using normal stress balance at the interface:

$$\left[\left(\tau^b_{yy}-\tau^a_{yy}\right)-\left(p^b-p^a\right)\right]\Big|_{y=0}=\sigma(T)\kappa, \tag{24}$$

where p is the pressure, κ is the curvature, and $\tau_{yy}=2\mu\partial v/\partial y$ is the normal stress. The curvature is taken to be positive if the center of curvature lies on the side of lower fluid, negative otherwise. To proceed, we need to calculate the pressure. This is done by writing equation (2) in its components forms in the x and y directions and integrating the resulting equations with respect to x and y, respectively. This procedure results in the following expressions for the pressure in the lower fluid

$$\frac{p^b(x,y)}{\mu_b U_{\max}k}=\frac{1}{\sin h^2(\beta)-\beta^2}\Big[-(\sin h(2\beta)-2\beta)\sin h(ky) -2\sin h^2(\beta)\cos h(ky)\Big]\cos(kx), \tag{25}$$

and the upper fluid

$$\frac{p^a(x,y)}{\mu_a U_{max}k}=\frac{1}{\sin h^2(\alpha)-\alpha^2}\Big[(\sin h(2\alpha)-2\alpha)\sin h(ky) -2\sin h^2(\alpha)\cos h(ky)\Big]\cos(kx), \tag{26}$$

respectively. Evaluations of equations (25) and (26) at $y=0$ yields the pressure jump at the interface

$$\frac{p^b-p^a}{\mu_b U_{\max}k}=2\left(\tilde{\mu}\frac{\sin h^2(\alpha)}{\sin h^2(\alpha)-\alpha^2}-\frac{\sin h^2(\beta)}{\sin h^2(\beta)-\beta^2}\right)\cos(kx). \tag{27}$$

Similarly, evaluation of τ_{xy} at $y=0$ yields the jump in the normal stresses at the interface

$$\frac{\tau^b_{yy}-\tau^a_{yy}}{\mu_b U_{\max}k}=2(\tilde{\mu}-1)\cos(kx). \tag{28}$$

In principal, it is possible to find the interface elevation along the channel, $y_i(x)$, by considering the variation of $\sigma(T)$ with x from equation (4), approximating $\kappa=y''_i/(1+y'^2_i)^{3/2}$ with $\kappa=y''_i$, and integration of the resulting expression for $y''_i\sim f(x)$ with respect to x. This procedure, however, does not lead to a closed form solution. To get around this, we assume that the interface elevation behaves according to $y_i=a_0\cos(kx)$, in line with the variations of the normal stresses and the pressures with x. Here, a_0 is the maximum deviation from the planar position. This allows us to find a_0 by balancing the coefficients of $\cos(kx)$ terms at both sides of equation (24). This assumption implies that the variation of $\sigma(T)$ with x is ignored in the course of calculation. However, once a_0 is found, the actual $\sigma(T)$ will be used in the expression for a_0. The above procedure yields

$$a_0=\frac{2U_{\max}}{\sigma(T)k}\left(\mu_a\frac{\alpha^2}{\sin h^2(\alpha)-\alpha^2}-\mu_b\frac{\beta^2}{\sin h^2(\beta)-\beta^2}\right). \tag{29}$$

The sense of interface deformation is determined by the sign of a_0 which in turn is set by the difference of the terms inside of the parentheses. Each term represents the product of the viscosity and a coefficient that is a function of the layer thickness. Since $\alpha+\beta=$ constant, when the nondimensional thickness of the lower fluid, β, is increased, the coefficient of μ_b increases while the coefficient of μ_a decreases. Since $y_i=a_0\cos(kx)$ and $\theta(x,y)=T_h+T_0\cos(kx)$, positive a_0 implies that the thickness of the lower layer is positively correlated with the temperature. This is an stabilizing effect as the higher (lower) film thickness at the place of higher (lower) wall temperature can reduce the heat flux. For liquid/liquid systems where μ_a and μ_b are of the same order, the relative thickness of the fluid layers is a determining factor in setting the sign of a_0. For fluids of nearly equal heights, a_0 is positive if the more viscous fluid would overlay on top of the less viscous fluids. For liquid/vapor systems where there is a large difference between the magnitude of μ_a and μ_b, the relative thicknesses of the fluids do not play a major role.

Fig. 7 shows the variation of interface height along the channel for two different systems. The interface height and the channel length are nondimensionalized by the channel length, l. Here, the nondimensional thicknesses of the fluid layers are $a/l=b/l=0.25$. The physical properties for both systems are those of the saturated liquid/vapor water at atmospheric pressure. For the first system, the vapor is overlaid on top of the liquid while for the second system the position of the liquid and the vapor is reversed. Here, $\tilde{k}=0.0365$ and $\tilde{\mu}=0.0431$ for the first system and $\tilde{k}=23.21$ and $\tilde{\mu}=27.42$ for the second one. The figure shows that the sense of interface deformation is opposite for the two systems and also the degree of deformation of the interface for the second system is about an order of magnitude less than that for the first system. The difference in the order of magnitudes is due to the reduction in $U_{\max}$ as a result of the poor heat transfer in the lower layer for the second system. In the context of micropatterned evaporators, the variation in the temperature of the lower wall can be interpreted as the variation in the elevation of an isothermal heated wall. As such, the sense of variation of the interface elevation for the first system, where $a_0<0$, suggests that the interface becomes thinner at the middle where the film thickness is already minimum. This implies

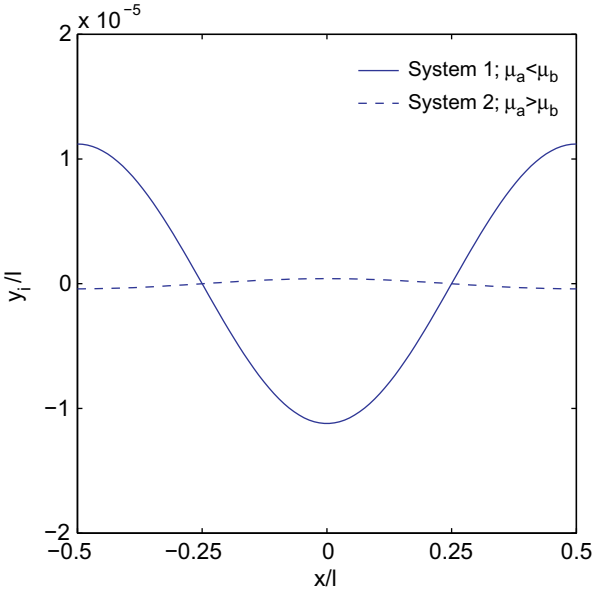

Fig. 7. Deviation of the interface from the planar shape along the channel for two different fluid systems. The physical properties correspond to saturate water at atmospheric pressure. For both cases, the thickness of the liquid layers are equal and the fluid properties are the same. However, for the first system, the vapor is overlaid on top of the liquid while the positions of the liquid and vapor are reversed for the second system.

that slight perturbations in the film thickness tends to destabilize the interface. The opposite is true for the second system.

7. Conclusions

Thermocapillary-driven fluid flow in a heated microchannel was investigated analytically in the limit of creeping flow and negligible heat convection. The channel was heated from below by imposing the top wall to a uniform temperature and the bottom wall to a sinusoidal temperature that was higher (on the average) than that of the top wall. The flow structure consisted of four counter-rotating vortices whose sizes in the vertical and horizontal directions were of the order of the thicknesses of the fluid layers, and half of the periodic length, respectively. For a given thicknesses of the fluid layers, the flow strength decreased with an increase in the thermal conductivity ratio, $\tilde{k} = k_a/k_b$, and the viscosity ratio, $\tilde{\mu} = \mu_a/\mu_b$. For a given system of fluids, the flow strength was maximum at a relative thickness of the fluid layers, a/b, which was set by competition between the thermal and the hydrodynamic effects. For small deformation, the distortion of interface was examined using normal stress jump condition and assuming that the interface height is $y_i = a_0 \cos(kx)$, where a_0 is the maximum deviation from the planar position. It was shown that the relative thickness of the fluid layers and the viscosity ratio set the sense of interface deformation. For fluids of equal heights, a_0 was positive (negative) if the more viscous fluid would overlay on top of the less (more) viscous fluids.

References

[1] A. Adamson, Physical Chemistry of Surfaces. John Wiley and Sons, New York, 1990.
[2] N.O. Young, J.S. Goldstein, M.J. Block, The motion of bubbles in a vertical temperature gradients. J. Fluid Mech. 6 (1959) 350–356.
[3] L.E. Scriven, V. Sterling, The Marangoni effects. Nature 187 (1960) 500–510.
[4] R.S. Subramanian, R. Balasubramaniam, The Motion of Bubbles and Drops in Reduced Gravity. Cambridge University Press, 2001.
[5] A.A. Darhuber, S.M. Troian, Principles of microfluidic actuation by modulation of surface stresses. Ann. Rev. Fluid Mech. 37 (2005) 425–455.
[6] J.P. Burelbach, S.G. Bankoff, S.H. Davis, Nonlinear stability of evaporating/condensing liquid film. J. Fluid Mech. 195 (1988) 463–494.
[7] S.W. Joo, S.H. Davis, S.G. Bankoff, Long-wave instabilities of heat falling films: two-dimensional theory of uniform layers. J. Fluid Mech. 230 (1991) 117–146.
[8] A. Oron, Nonlinear dynamics of three-dimensional long-wave Marangoni instability in thin liquid films. Phys. Fluids 12 (2000) 1633–1645.
[9] D. Erickson, D. Li, Microchannel flow with patchwise and periodic surface heterogeneity. Langmuir 18 (2002) 8949–8959.
[10] H.A. Stone, A.D. Stroock, A. Ajdari, Engineering flows in small devices: micorfluidics toward a lab-on-chip. Ann. Rev. Fluid Mech. 36 (2004) 381–411.
[11] Y. Fujita, Boiling and evaporation of falling film on horizontal tubes and its enhancement on grooved tubes. in: S. Kakac, A.E. Bergles, F. Mayinger, H. Yunch (Eds.), Heat Transfer Enhancement of Heat Exchangers. Kluwer Academic Publishers, Dordrecht, The Netherlands, 1998, pp. 325–346.